

Kinetic multiscale scheme based on the discrete-velocity and lattice-Boltzmann methods

V.V. Aristov^a, O.V. Ilyin^a, O.A. Rogozin^{b,a,*}

^a*Dorodnicyn Computing Center, Federal Research Center "Computer Science and Control" of Russian Academy of Science, Moscow, Russia*

^b*Center for Design, Manufacturing, and Materials, Skolkovo Institute of Science and Technology, Moscow, Russia*

Abstract

A novel hybrid computational method based on the discrete-velocity (DV) approximation, including the lattice-Boltzmann (LB) technique, is proposed. Numerical schemes for the kinetic equations are used in regions of rarefied flows, and LB schemes are employed in continuum flow zones. The schemes are written under the finite-volume (FV) formulation to achieve the flexibility of local mesh refinement. The truncated Hermite polynomial expansion is used for matching of DV and LB solutions. Special attention is paid to preserving conservation properties in the coupling algorithm. The test results obtained for the Couette flow of a rarefied gas are in excellent agreement with the benchmark solutions, mostly thanks to mesh refinement (both in the physical and velocity spaces) in the Knudsen layer.

Keywords: hybrid numerical method, discrete-velocity method, lattice-Boltzmann method, domain decomposition, Knudsen layer.

Contents

1	Introduction	2
2	Main equations	3
3	Discrete-velocity approximation	4
4	The mapping method	6
5	Numerical method	7
5.1	Time-integration method	7
5.2	Finite-volume formulation	7
5.3	Coupling algorithm	9
5.4	Mesh refinement	10
6	Results and discussion	10
6.1	Couette-flow problem	10
6.2	Numerical analysis	11
6.3	Breakdown criterion	16
7	Conclusions and perspectives	18

*Corresponding author
Email address: oleg.rogozin@phystech.edu (O.A. Rogozin)

Appendix A	Third-order TVD limiter for the FV scheme	18
Appendix B	Solution of the linear Couette-flow problem for the BGK model	19

1. Introduction

Thus far, effective numerical simulation of multiscale flows has remained a challenging problem despite the efforts of many researchers. This is due, in particular, to complicated flow structures, where small-scale highly nonequilibrium regions coexist with large-scale equilibrium zones. The use of the kinetic equation in all regions is very demanding from a computational point of view. On the other hand, the fluid-dynamics models provide an efficient approximation of near-equilibrium flows, but this kind of description is not adequate in regions where the velocity distribution function (VDF) is far from the Maxwellian and the contribution of high moments cannot be neglected.

There are two main approaches on how to deal with the multiscale problems [1]. The first one employs different kinds of representations for equilibrium and nonequilibrium parts of the solution in the entire computational space, while the second one handles the problem by dividing the physical domain into the highly rarefied and near-equilibrium regions using some criterion of domain decomposition. The fluid-kinetic coupling is a natural and effective approach for the description of multiscale flows. Coupling of the Boltzmann and Euler or Navier–Stokes (NS) equations is a canonical example of such hybrid schemes [2, 3].

The numerical schemes based on the kinetic description of the fluid and capable of reproducing the Euler and NS dynamics have been suggested independently and widely used since the early 1980s [4, 5, 6, 7]. Later these pioneer kinetic schemes have been significantly developed in [8, 9, 10, 11, 12, 13, 14]. The cellular-automata approximation for the NS equations was developed in the middle of the 80s [15]. Finally, the lattice-gas model based on the BGK equation was proposed at the beginning of the 90s [16]. It gave rise to a broad class of numerical methods called lattice-Boltzmann (LB) methods [17, 18, 19].

The LB models can be roughly divided into two classes: low-order and high-order. The low-order LB models recover the correct hydrodynamics for small Mach numbers, while the high-order models are able to reproduce full Navier–Stokes–Fourier equations and, moreover, some rarefied-gas effects [19, 20]. The LB method is a flexible framework for developing sophisticated models. Many recent works are devoted to extending the applicability of the LB method beyond the Navier–Stokes level. In particular, models that correctly describe the Burnett-level dynamics is formulated in [21, 22]. Special-purpose methodologies are proposed to capture rarefied-gas effects in the highly nonequilibrium Knudsen layer arising from the kinetic boundary conditions [23, 24, 25, 26]. Another promising approach is based on the regularization procedure for LB models [27].

It is worth emphasizing that there is a fundamental relationship between the LB and DV methods. For instance, one can cite a phrase from [28]: “This type of discrete kinetic theory can be seen as the ancestor of the lattice gas approach.” The LB method is genetically related to the Broadwell-type models [29, 30], which use a small number of discrete velocities to reproduce some relevant features of the Boltzmann equation. The DV method typically uses lattices with a large number of discrete velocities, which can accurately approximate highly nonequilibrium VDF. In contrast, discontinuities and sharp variations of the VDF cannot be reproduced on a span of the truncated basis of smooth polynomials underlying the LB models.

The idea of coupling the low-order and high-order LB models is presented in [31]. The hybrid approach based on the DSMC and LB methods is proposed in [32, 33]. Unlike DSMC, the deterministic methods for solving the Boltzmann equation do not produce statistical noise. Therefore, hybrid approaches based on them appear to be more promising. The possibility of merging the DV and LB methods is noticed in [34], while the first results based on matching of the half-range fluxes have been presented in [35].

The proposed hybrid kinetic approach is based on coupling the DV and LB methods. The DV method accurately describes nonequilibrium regions, while the LB method provides an efficient approximation in the continuum regions. To couple solutions between the DV and LB subdomains, the VDF is projected onto the truncated Hermite basis in the buffer zone. The kinetic breakdown criterion determines the position of the coupling interface. The first implementation of this method is reported in [36]. In the present paper,

the accuracy of the method has been significantly improved by employing nonuniform grids for the DV approximation in the Knudsen layer.

The classical LB methods enjoy their efficiency coming from the highly symmetric discrete physical space and time. However, uniform Cartesian meshes lack flexibility and, therefore, local mesh refinement. There are several approaches how to work around this limitation. The LB method is easily extended for arbitrary unstructured meshes under the FV formulation [37, 38, 39, 40]. In the present paper, this strategy is adopted, specifically to refine mesh near the boundary.

Ideologically, the present work is similar to the works [32, 33], but there is a significant difference. The proposed hybrid approach is based on the unified DV approximation, whereas the DSMC method has a fundamentally different representation of the VDF. In this sense, coupling DV and LB models under the single FV formulation is more natural.

The plan of the present paper is as follows. The governing equations and nondimensional variables are introduced in Sec. 2. The DV approximation of the VDF underlying both DV and LB method is outlined in 3. The mapping method between DV and LB models is described in Sec. 4. Details of the numerical schemes and algorithms are presented in Sec. 5. Numerical solutions of the Couette-flow problem are obtained by the DV model, various LB models, and their hybrid combinations. They are illustrated and compared with each other for various Knudsen numbers in Sec. 6. Possible equilibrium breakdown parameters and computational efficiency of the hybrid approach is also analyzed in Sec. 6. Perspectives of the kinetic multiscale methods based on coupling the DV and LB solutions are discussed in Sec. 7. The peculiar details of the finite-volume scheme are included in Appendix A. Finally, a set of supplementary formulas for the benchmark solution of the linear Couette-flow problem, which is used to validate the investigated numerical methods, is provided in Appendix B.

2. Main equations

We first introduce the notation for describing a dilute gas. Let L , ρ_0 , T_0 , $c_0 = \sqrt{RT_0}$ and $p_0 = \rho_0 RT_0$ be the reference length, density, temperature, velocity, and pressure, respectively. The specific gas constant $R = k_B/m$, where k_B is the Boltzmann constant, and m is the molar mass. Then, $f\rho_0/c_0^3$ is the one-particle velocity distribution function (VDF) defined in seven-dimensional space $(tL/c_0, \mathbf{x}L, \boldsymbol{\xi}c_0)$ and the macroscopic variables take the following form: $\rho\rho_0$ is the density, $\mathbf{v}c_0$ is the velocity, TT_0 is the temperature, $p_{\alpha\beta}p_0$ is the stress tensor, $\mathbf{q}p_0c_0$ is the heat flux. In the dimensionless form, they are calculated as polynomial moments of the VDF:

$$\begin{aligned} \rho &= \int f d\boldsymbol{\xi}, \quad \mathbf{v} = \frac{1}{\rho} \int \boldsymbol{\xi} f d\boldsymbol{\xi}, \quad T = \frac{1}{3\rho} \int |\boldsymbol{\xi} - \mathbf{v}|^2 f d\boldsymbol{\xi} = \frac{p_{\alpha\alpha}}{3\rho}, \\ p_{\alpha\beta} &= \int (\xi_\alpha - v_\alpha)(\xi_\beta - v_\beta) f d\boldsymbol{\xi}, \quad \mathbf{q} = \frac{1}{2} \int (\boldsymbol{\xi} - \mathbf{v}) |\boldsymbol{\xi} - \mathbf{v}|^2 f d\boldsymbol{\xi}. \end{aligned} \quad (1)$$

Integration with respect to $\boldsymbol{\xi}$ is, hereafter, carried out over \mathbb{R}^3 .

The VDF is governed by the Boltzmann equation

$$\frac{\partial f}{\partial t} + \boldsymbol{\xi} \cdot \frac{\partial f}{\partial \mathbf{x}} = \frac{1}{\tau} J(f), \quad (2)$$

where $J(f)$ is the collisional operator with a local Maxwellian as the equilibrium function

$$f^{(\text{eq})}(\boldsymbol{\xi}; \rho, \mathbf{v}, T) = \frac{\rho}{(2\pi T)^{3/2}} \exp\left(-\frac{|\boldsymbol{\xi} - \mathbf{v}|^2}{2T}\right). \quad (3)$$

The characteristic relaxation time of collisions to equilibrium τ can be expressed in terms of the reference gas viscosity μ_0 [41, 42],

$$\tau = \frac{\mu_0 c_0}{p_0 L}, \quad (4)$$

and is related to the modified Knudsen number $k = \ell_0 \sqrt{\pi}/2L$, where ℓ_0 is the mean free path, as $\tau = k/\sqrt{2}$.

In the present paper, we restrict ourselves to the simplest relaxation model [43, 44]

$$J(f)(\boldsymbol{\xi}) = f^{(\text{eq})}(\boldsymbol{\xi}) - f(\boldsymbol{\xi}), \quad (5)$$

often referred as the Bhatnagar–Gross–Krook (BGK) model of the Boltzmann collisional operator. The nonlinearity in (5) is more severe in comparison to the full Boltzmann equation since $f^{(\text{eq})}$ depends on f via its moments, but the BGK model is much simpler from the numerical point of view.

The gas–surface interaction is modeled via the diffuse-reflection boundary condition:

$$f(t, \mathbf{x}_B, \boldsymbol{\xi}) = f^{(\text{eq})} \left(\boldsymbol{\xi}; -\sqrt{\frac{2\pi}{T_B}} \int_{\boldsymbol{\xi}' \cdot \mathbf{n} < 0} (\boldsymbol{\xi}' \cdot \mathbf{n}) f(t, \mathbf{x}_B, \boldsymbol{\xi}') d\boldsymbol{\xi}', \mathbf{v}_B, T_B \right) \quad (\boldsymbol{\xi} \cdot \mathbf{n} > 0), \quad (6)$$

where \mathbf{n} is the unit vector normal to the boundary, directed into gas, \mathbf{x}_B , T_B , and \mathbf{v}_B are the boundary coordinates, temperature, and velocity, respectively. It is also assumed that $\mathbf{v}_B \cdot \mathbf{n} = 0$.

3. Discrete-velocity approximation

Within the DV framework, the admissible particle velocities are restricted to the discrete set $\{\boldsymbol{\xi}_j : j = 1, \dots, N\}$. Under this assumption, an arbitrary moment $\phi(\boldsymbol{\xi})$ of f , including (1), is approximated as

$$\int \phi f d\boldsymbol{\xi} = \sum_{j=1}^N \phi(\boldsymbol{\xi}_j) f_j, \quad (7)$$

where f_j/w_j is an approximation of $f(\boldsymbol{\xi}_j)$, w_j is a quadrature weight. The evolution of f_j is governed by the system of partial differential equations

$$\frac{\partial f_j}{\partial t} + \boldsymbol{\xi}_j \cdot \frac{\partial f_j}{\partial \mathbf{x}} = \frac{1}{\tau} J_N(f_j) \quad (8)$$

which is called the DV model of (2) [45]. The *DV method* of solving (2) is based on a DV model, which is consistent with (2) when N goes to infinity [46].

It is important for a DV model (8) to preserve conservation and entropy properties of the continuous kinetic equation (2). For the BGK model

$$J_N(f_j) = f_j^{(\text{eq})} - f_j, \quad (9)$$

it can be accomplished when the discrete local equilibrium $f_j^{(\text{eq})}$ has the Maxwellian form

$$f_{\text{DV},j}^{(\text{eq})}(\hat{\mathbf{m}}) = \frac{\hat{\rho} w_{\text{DV},j}}{(2\pi \hat{T})^{3/2}} \exp\left(-\frac{|\boldsymbol{\xi}_{\text{DV},j} - \hat{\mathbf{v}}|^2}{2\hat{T}}\right), \quad \hat{\mathbf{m}} = (\hat{\rho}, \hat{\mathbf{v}}, \hat{T})^\top \in \mathbb{R}^5, \quad (10)$$

where vector $\hat{\mathbf{m}}$ is the solution of

$$\sum_j \boldsymbol{\psi}_{\text{DV},j} \left(f_{\text{DV},j}^{(\text{eq})}(\hat{\mathbf{m}}) - f_j \right) = 0, \quad \boldsymbol{\psi}_j = (1, \boldsymbol{\xi}_j, |\boldsymbol{\xi}_j|^2)^\top \in \mathbb{R}^5. \quad (11)$$

For a uniform lattice in the velocity space, it is proved that there exists a unique discrete equilibrium (10), which is the maximization of the discrete entropy functional and guarantees that mass, momentum, and kinetic energy are conserved [47]. For computations, a finite number of discrete velocities is used: $N = N_{\text{DV}} < \infty$. Note also that moments of (10) are not associated with $\hat{\mathbf{m}}$:

$$\sum_j \boldsymbol{\psi}_{\text{DV},j} f_{\text{DV},j}^{(\text{eq})}(\hat{\mathbf{m}}) = \rho(1, \mathbf{v}, |\mathbf{v}|^2 + 3T)^\top, \quad \mathbf{m} = (\rho, \mathbf{v}, T)^\top \in \mathbb{R}^5. \quad (12)$$

Vector \mathbf{m} is not equal to $\hat{\mathbf{m}}$, but is quite close to it in practice, when the velocity grid is well suited to the problem.

When the velocity grid is anisotropic, the diagonal terms of the pressure tensor $p_{\alpha\beta}$ calculated from $f_{\text{DV},j}^{(\text{eq})}$ are not in general equal to each other. Hence, the discrete equilibrium (10) has at least a direction-dependent momentum flux $p_{\alpha\beta}n_\alpha \neq \rho T n_\beta$ across an arbitrary interface with unit normal \mathbf{n} . Thus, 5-moment Maxwellian (10) is sufficient to construct the conservative DV method even for nonuniform anisotropic grids in the velocity space, but not for hybrid numerical method based on coupling of DV approximations with different degrees of $p_{\alpha\beta}$ anisotropy. This anisotropy can be eliminated if the discrete equilibrium is constructed in the form

$$f_{\text{DV},j}^{(\text{eq})}(\hat{\mathbf{m}}) = \hat{\rho} w_{\text{DV},j} \prod_{\alpha} \left(2\pi \hat{T}_{\alpha} \right)^{-1/2} \exp \left(- \sum_{\alpha} \frac{(\xi_{\text{DV}\alpha,j} - \hat{v}_{\alpha})^2}{2\hat{T}_{\alpha}} \right), \quad \hat{\mathbf{m}} = (\hat{\rho}, \hat{\mathbf{v}}, \hat{\mathbf{T}})^{\text{T}} \in \mathbb{R}^7, \quad (13)$$

where $\xi_{\text{DV}\alpha,j} \equiv \xi_{\text{DV},j}$, vector $\hat{\mathbf{m}}$ is the solution of

$$\sum_j \psi_{\text{DV},j} \left(f_{\text{DV},j}^{(\text{eq})}(\hat{\mathbf{m}}) - f_j \right) = 0, \quad \psi_j = (1, \xi_j, \xi_j^2)^{\text{T}} \in \mathbb{R}^7. \quad (14)$$

The 7-moment Maxwellian (13) can also be obtained from generalized minimum entropy principle [48].

The *LB method* can be considered as a special discretization of the BGK model [19, 49]. We assume that the considered flow is isothermal and slow, i.e., the Mach number is close to zero. Then we can expand the local Maxwell state into the Taylor series on the bulk velocity \mathbf{v} and keep only the terms of some finite order (at least second). Moreover, we assume that the particle can travel with the velocities $\xi_{\text{LB},j}, j = 1 \dots N_{\text{LB}}$. The values of absolute Maxwellian are changed by the lattice weights $w_{\text{LB},j}$ in such a way that the first moments of the local equilibrium state are the same as for the Maxwell distribution. For the LB models, the local equilibrium takes a polynomial form on the bulk velocity, and the requirement of the conservation of mass, momentum, and energy yields the algebraic equations for the lattice weights and velocities, which can be solved explicitly. Therefore the conservation properties for LB method are achieved with much less efforts than for the conventional DV method.

The third-order expansion in \mathbf{v} yields the following local equilibrium LB state:

$$f_{\text{LB},j}^{(\text{eq})}(\mathbf{m}) = \rho w_{\text{LB},j} \left(1 + \frac{\xi_{\text{LB},j} \cdot \mathbf{v}}{c_s^2} + \frac{(\xi_{\text{LB},j} \cdot \mathbf{v})^2 - c_s^2 v^2}{2c_s^4} + \frac{(\xi_{\text{LB},j} \cdot \mathbf{v})^3 - 3c_s^2 v^2 (\xi_{\text{LB},j} \cdot \mathbf{v})}{6c_s^6} \right), \quad (15)$$

where c_s is the constant sound velocity defined by $\sum_j w_j \xi_{\text{LB},j}^2 = 3c_s^2$. In the present study, the value of c_s is calibrated to unity for all LB models. The standard notation D3Q p means $N_{\text{LB}} = p$ for the three-dimensional LB model. In the case of low-order lattices like D3Q19, the third-order terms are truncated in (15). Hereinafter, a quadrature rule, based on $\xi_{\text{LB},j}$ and $w_{\text{LB},j}$, together with the discrete operator in form (15), is referred to as the LB model.

When the VDF is a slightly disturbed equilibrium, it can be efficiently approximated using quadratures with a small number N_{LB} . The LB models are capable of reproducing low-order polynomial moments of the VDF accurately and, therefore, describing a fluid-dynamic behavior of a gas, including that beyond the NS level. Several approaches can be applied for the construction of LB models like Gauss–Hermite [50, 51, 20, 52] and the entropic method [53, 54, 55].

The diffuse-reflection boundary condition (6) is discretized as

$$f_j(t, \mathbf{x}_B) = - \frac{\sum_{\xi_k \cdot \mathbf{n} < 0} (\xi_k \cdot \mathbf{n}) f_k(t, \mathbf{x}_B)}{\sum_{\xi_k \cdot \mathbf{n} > 0} (\xi_k \cdot \mathbf{n}) f_k^{(\text{eq})}(\mathbf{m}_B)} f_j^{(\text{eq})}(\mathbf{m}_B) \quad (\xi_j \cdot \mathbf{n} > 0), \quad \mathbf{m}_B = (1, \mathbf{v}_B, T_B)^{\text{T}}, \quad (16)$$

which preserves conservation of mass.

4. The mapping method

We will introduce the mapping method in the spatial overlapping zone of the BGK and LB models. First of all, we assume that in this domain the VDF of the gas is close to the Maxwell state with zero bulk velocity and unit temperature. Therefore, VDF can be represented in the form of the truncated Grad expansion up to the third-order terms on the velocity

$$f_H(\mathbf{x}, \boldsymbol{\xi}) = \omega(\boldsymbol{\xi}) \left(a(\mathbf{x}) + \sum_{\alpha} a_{\alpha}(\mathbf{x}) H_{\alpha} + \frac{1}{2!} \sum_{\alpha\beta} a_{\alpha\beta}(\mathbf{x}) H_{\alpha\beta} + \frac{1}{3!} \sum_{\alpha\beta\gamma} a_{\alpha\beta\gamma}(\mathbf{x}) H_{\alpha\beta\gamma} \right), \quad (17)$$

where $H_{\alpha}, H_{\alpha\beta}, H_{\alpha\beta\gamma}$ are the Hermite polynomials of the first, second, and third order (in the case of low-order LB models only the terms up to the second order are retained). The polynomials are defined by

$$H_{\alpha}(\boldsymbol{\xi}) = \frac{(-1)}{\omega(\boldsymbol{\xi})} \frac{\partial}{\partial \xi_{\alpha}} \omega(\boldsymbol{\xi}), \quad H_{\alpha\beta}(\boldsymbol{\xi}) = \frac{1}{\omega(\boldsymbol{\xi})} \frac{\partial^2}{\partial \xi_{\alpha} \partial \xi_{\beta}} \omega(\boldsymbol{\xi}), \quad H_{\alpha\beta\gamma}(\boldsymbol{\xi}) = \frac{(-1)}{\omega(\boldsymbol{\xi})} \frac{\partial^3}{\partial \xi_{\alpha} \partial \xi_{\beta} \partial \xi_{\gamma}} \omega(\boldsymbol{\xi}), \quad (18)$$

and

$$\omega(\boldsymbol{\xi}) = \frac{1}{(2\pi)^{3/2}} \exp\left(-\frac{\boldsymbol{\xi}^2}{2}\right). \quad (19)$$

The coefficients $a, a_{\alpha}, a_{\alpha\beta}, a_{\alpha\beta\gamma}$ depend on \mathbf{x} (the point in the overlapping domain). We will use the function (17) for the transfer of the data between the LB and the BGK models.

In the overlapping spatial domain, where two methods (LB and DV) are applied, one needs to introduce the procedure of the data exchange between LB and DV methods. It consists of two parts: the mapping from DV to LB and the mapping from LB to DV. These steps are discussed below.

DV to LB. Similarly to [32], this step can be termed as *projection*, since the DV VDF, which contains information about all the moments, is mapped on LB VDF, which describes correctly only some low-order moments.

Firstly, in the overlapping spatial domain (physical domain), we map the DV VDF on the Grad VDF by calculating the following coefficients:

$$a = \sum_{j=1}^{N_{DV}} f_{DV,j}, \quad a_{\alpha} = \sum_{j=1}^{N_{DV}} f_{DV,j} H_{\alpha}(\boldsymbol{\xi}_{DV,j}), \quad a_{\alpha\beta} = \sum_{j=1}^{N_{DV}} f_{DV,j} H_{\alpha\beta}(\boldsymbol{\xi}_{DV,j}), \quad a_{\alpha\beta\gamma} = \sum_{j=1}^{N_{DV}} f_{DV,j} H_{\alpha\beta\gamma}(\boldsymbol{\xi}_{DV,j}).$$

Now the Grad VDF (17) is recovered in the overlapping spatial domain.

Next, we will map (17) on the LB distribution function using the Gauss–Hermite quadrature method. The idea of the method is based on the fact that the representation of the VDF in the Grad form is equivalent to the LB method [50, 51, 20]. Then the formula

$$f_{LB,j} = w_j \frac{f_H(\boldsymbol{\xi}_{LB,j})}{\omega(\boldsymbol{\xi}_{LB,j})} \quad (20)$$

gives the mapping of f_H to $f_{LB,j}$.

LB to DV. Following [32], this step can be termed as *reconstruction*, since one needs to find DV VDF having only the LB VDF, which has less information about the moments than DV VDF.

Using LB VDF we evaluate the moments $a, a_{\alpha}, a_{\alpha\beta}, a_{\alpha\beta\gamma}$ using the formulas

$$a = \sum_{j=1}^{N_{LB}} f_{LB,j}, \quad a_{\alpha} = \sum_{j=1}^{N_{LB}} f_{LB,j} H_{\alpha}(\boldsymbol{\xi}_{LB,j}), \quad a_{\alpha\beta} = \sum_{j=1}^{N_{LB}} f_{LB,j} H_{\alpha\beta}(\boldsymbol{\xi}_{LB,j}), \quad a_{\alpha\beta\gamma} = \sum_{j=1}^{N_{LB}} f_{LB,j} H_{\alpha\beta\gamma}(\boldsymbol{\xi}_{LB,j})$$

and recover Grad distribution function (17). Finally, the DV VDF is obtained by appropriate discretization of the Grad VDF.

The described mapping method can be generalized for the LB models, which are not derived from the Gauss–Hermite quadratures. We assume that after the regularization procedure [56, 57] and [58, 27, 59], the non-equilibrium part of LB VDF will be projected into a velocity space with a basis spanned by Hermite polynomials of the appropriate order. Then the equivalence between the LB VDF and the expansion of the Grad type can be achieved; therefore, the proposed mapping method can be applied.

5. Numerical method

5.1. Time-integration method

For the present study, we start from the straightforward numerical algorithm providing the second-order accuracy for both time and physical coordinates. Equation (2) is solved by the symmetric Strang’s splitting scheme

$$S_{A+B}^{\Delta t}(f_0) = S_A^{\Delta t/2} \left(S_B^{\Delta t} \left(S_A^{\Delta t/2}(f_0) \right) \right) + O(\Delta t^3), \quad (21)$$

where $A(f) = -\boldsymbol{\xi} \cdot \nabla f$, $B(f) = J(f)/\tau$, Δt is the time step. $S_P^t(f_0)$ denotes the solution of the Cauchy problem

$$\frac{\partial f}{\partial t} = P(f), \quad f|_{t=0} = f_0. \quad (22)$$

Scheme (21) preserves the second-order accuracy if S_A^t and S_B^t are approximated with the same convergence properties individually [60].

An essential advantage of the splitting procedure is that the spatially homogeneous Boltzmann equation has an exact solution for the BGK collision model:

$$S_B^t(f_0) = f^{(\text{eq})} + \left(f_0 - f^{(\text{eq})} \right) \exp\left(-\frac{\rho}{\tau} t\right); \quad (23)$$

however, the generalization to the original Boltzmann equation is straightforward. For the collisionless Boltzmann equation, the desired second-order accuracy of $S_A^t(f_0)$ is archived by means of the finite-volume scheme described below.

To find a steady-state solution of the boundary-value problem, the time-marching process is started from some initial approximation and continues until the convergence criterion is met. For the DV method, the discrete equilibrium $f_{\text{DV},j}^{(\text{eq})}$ is obtained as a solution of the nonlinear equations (11) or (14) at each time step. For this purpose, some root-finding algorithm should be harnessed.

5.2. Finite-volume formulation

For the sake of simplicity, we consider a one-dimensional physical space and introduce $\boldsymbol{\xi} = \boldsymbol{\xi}_1$, $x = x_1$. Then, the collisionless Boltzmann equation with discrete velocities

$$\frac{\partial f(\boldsymbol{\xi}_j)}{\partial t} + \boldsymbol{\xi}_j \frac{\partial f(\boldsymbol{\xi}_j)}{\partial x} = 0 \quad (24)$$

is approximated by the finite-volume (FV) method:

$$f_m^{n+1} = f_m^n - \gamma_m \left(f_{m+1/2}^{n+1/2} - f_{m-1/2}^{n+1/2} \right), \quad \gamma_m(\boldsymbol{\xi}_j) = \frac{\boldsymbol{\xi}_j \Delta t}{\Delta x_m}, \quad m = 1, \dots, M, \quad n \in \mathbb{N}, \quad (25)$$

where Δx_m is the width of m cell in the physical space ($\boldsymbol{x} \in \mathbb{R}$), $f_m^n(\boldsymbol{\xi}_j)$ denotes the fully discretized VDF defined in the cell centers:

$$f_m^n(\boldsymbol{\xi}_j) = f \left(t = t_n \equiv n\Delta t, x = x_m \equiv \frac{\Delta x_m}{2} + \sum_{l=1}^{m-1} \Delta x_l, \boldsymbol{\xi} = \boldsymbol{\xi}_j \right) \quad (26)$$

and $f_{m+1/2}^{n+1/2}(\boldsymbol{\xi}_j)$ ($m = 0, \dots, M$) are the reconstructed edge values defined at $x_{m+1/2} = \sum_{l=0}^m \Delta x_l$. The computational domain $\Omega = [0, L]$, where $L = x_{M+1/2}$, is extended by two ghost cells, which are corresponded

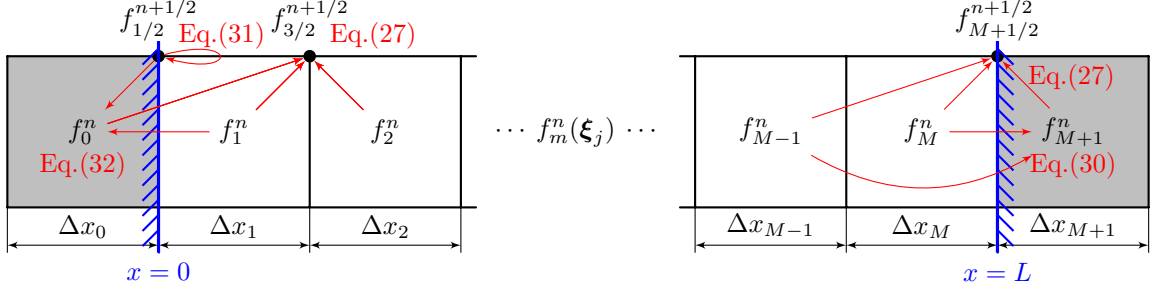


Figure 1: The computational domain $\Omega = [0, L]$ is extended by two ghost cells (shown in gray). The blue lines highlight the boundaries of Ω . The red arrows represent the dependency relations among the set of nodes in the extended Ω for $\xi_j > 0$. The values in nodes pointed out by these arrows are calculated from the provided references.

to $m = 0$ and $m = M + 1$ (Fig. 1). Hereinafter, we describe only positive velocities $\xi_j > 0$. Fig. 1 shows a mesh with two ghost cells at each boundary. For $\xi_j < 0$, all expressions are analogous and can be obtained by the replacement $\xi_j \rightarrow -\xi_j$ and $x \rightarrow -x$.

The internal edge values can be written in the form

$$f_{m+1/2}^{n+1/2} = f_m^n + \frac{1 - \gamma_m}{2} \overline{Df_m^n} \Delta x_m, \quad m = 1, \dots, M, \quad (27)$$

where $\overline{Df_m^n}$ is the limited approximation of $\partial f / \partial x(t_n, x_m, \xi_j)$. A monotonic-preserve scheme should be employed because sharp variations (in physical space) of solution can occur even for nearly incompressible flow, especially for large $|\xi_j|$. In the present paper, the third-order total variation diminishing (TVD) scheme is used (see Appendix A for details):

$$\overline{Df_m^n} = \begin{cases} \min\left(\frac{2}{\gamma_m} \frac{|\Delta_-|}{h_-}, \frac{1+\gamma_m}{3} \frac{|\Delta_-|}{h_-} + \frac{2-\gamma_m}{3} \frac{|\Delta_+|}{h_+}, \frac{2}{1-\gamma_m} \frac{|\Delta_+|}{h_+}\right) \text{sgn}(\Delta_-), & \Delta_+ \Delta_- > 0, \\ 0, & \Delta_+ \Delta_- \leq 0, \end{cases} \quad (28)$$

where

$$\Delta_{\pm} = \pm(f_{m\pm 1}^n - f_m^n), \quad h_{\pm} = \frac{\Delta x_{m\pm 1} + \Delta x_m}{2}. \quad (29)$$

The outflow boundary condition are expressed in terms of edge values $f_{M+1/2}^{n+1/2}(\xi_j)$, which are obtained from (27) and the linear extrapolation for the ghost cell $m = M + 1$:

$$f_{M+1}^n = 2f_M^n - f_{M-1}^n, \quad \Delta x_{M+1} = \Delta x_{M-1}, \quad (30)$$

which preserve the second-order accuracy [61]. The inflow boundary condition is included into the scheme by means of $f_{1/2}^{n+1/2}$ and $f_{3/2}^{n+1/2}$. In particular, the DV diffuse-reflection boundary condition (16) yields

$$f_{1/2}^{n+1/2}(\xi_j) = -\frac{\sum_{\xi_k > 0} \xi_k f_{1/2}^{n+1/2}(\xi_k)}{\sum_{\xi_k < 0} \xi_k f_k^{(\text{eq})}(\mathbf{m}_B)} f_j^{(\text{eq})}(\mathbf{m}_B). \quad (31)$$

For the ghost cell $m = 0$, used for calculation $f_{3/2}^{n+1/2}$ via (27), the linear extrapolation of the form

$$f_0^n = \frac{2}{1 + \gamma_1} f_{1/2}^{n+1/2} - \frac{1 - \gamma_1}{1 + \gamma_1} f_1^n, \quad \Delta x_0 = \Delta x_1 \quad (32)$$

also preserves the second-order accuracy, since it is a linear extrapolation of two values at $t = t_n$: f_1^n and $f_{1/2}^{n+1/2} \equiv f(t_n + \Delta t/2, 0, \xi_j) = f(t_n, -\gamma_1 \Delta x_1/2, \xi_j)$. It is worth emphasizing that the presented numerical

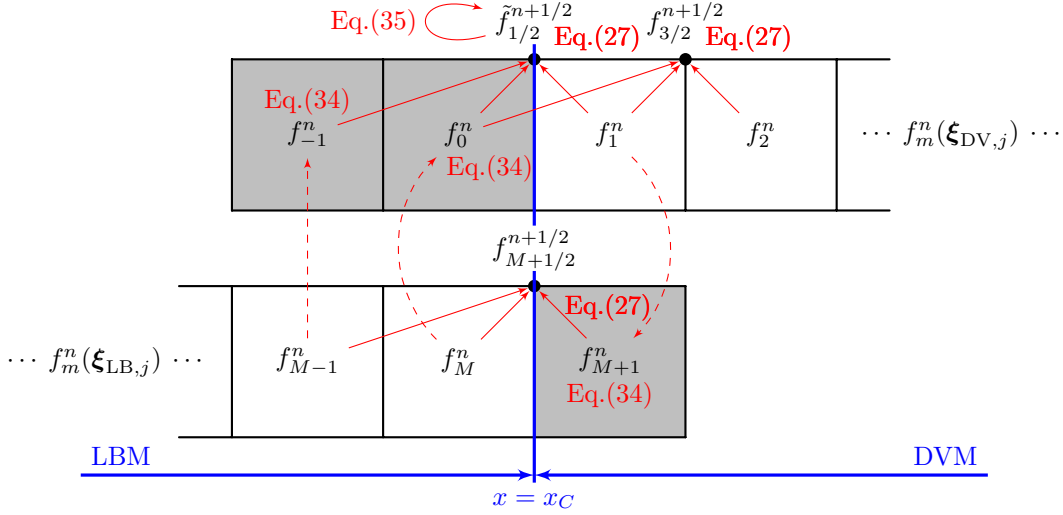


Figure 2: The computational domain Ω is divided into LB and DV subdomains, which are extended by the ghost cells (shown in gray). The vertical blue line highlight the coupling interface $x = x_C$. The red arrows represent the dependency relations among the set of nodes in the extended Ω for $\xi_j > 0$. The values in nodes pointed out by these arrows are calculated from the provided references. The dashed red arrows correspond to the projection of the solution onto the truncated Hermite basis.

scheme for the boundary-value problem possesses the second-order accuracy along with conservation of mass (in contrast to the FV scheme used in [62]).

The maximum value of the time step Δt for the described explicit scheme is limited by the Courant–Friedrichs–Lewy (CFL) condition: $\gamma_m(\xi_j) \leq 1$ for all m and j , which is equivalent to

$$\Delta t \leq \min_{m,j} \frac{\Delta x_m}{\xi_j}. \quad (33)$$

The boundary conditions also dictate a way of discretization in the velocity space. Concerning the origin of the velocity coordinates, only two types of lattices are symmetric [63]: integer $(\xi_j/c_s) \in \mathbb{Z}^3$ and half-integer $(\xi_j/c_s + e/2) \in \mathbb{Z}^3$, where e is the corresponding orthonormal basis. For the considered boundary condition at $x = 0$, there is a zero-measure set of velocities $\{\xi \in \mathbb{R}^3 : \xi_1 = 0\}$, called tangential. These velocities are immune to the boundary conditions. The integer lattice contains a substantial subset of tangential velocities. Therefore, to avoid an additional discretization error, the half-integer lattice is employed.

In the same manner, LB quadratures without tangential velocities are preferable to the classical ones. The LB models can be supplemented by special velocity groups to more accurately approximate the diffuse-reflection boundary condition by minimizing errors at the half-space moments [23]. Moreover, the Gauss–Laguerre quadratures are able to reproduce the Maxwell half-range moments exactly [24, 25].

5.3. Coupling algorithm

The mapping approach presented in Sec. 4 can be implemented within the FV framework. Let us divide our physical domain into the LB and DV subdomains. The coupling condition at the interface between these subdomains can be represented as a virtual boundary condition. The proposed coupling strategy is based on the concept of ghost cells, in which the VDF is reconstructed from the truncated Hermite expansion (17):

$$f_j^{(H)} = f_j^{(eq)}(\mathbf{m}_0) \left(a + \sum_{\alpha} a_{\alpha} H_{\alpha}(\xi_j) + \frac{1}{2} \sum_{\alpha,\beta} a_{\alpha\beta} H_{\alpha\beta}(\xi_j) + \frac{1}{6} \sum_{\alpha,\beta,\gamma} a_{\alpha\beta\gamma} H_{\alpha\beta\gamma}(\xi_j) \right), \quad (34)$$

where $\mathbf{m}_0 = (1, \mathbf{0}, 1)^{\top}$, $f_{LB,j}^{(eq)}(\mathbf{m}_0) = w_{LB,j}$, which is seen from (15), and $f_{DV,j}^{(eq)}(\mathbf{m}_0)$ is close to $w_{DV,j}\omega(\xi_{DV,j})$, but not equal to it for the conservative DV method.

Let us return to the one-dimensional case described in Sec. 5.2 and suppose that $x = x_C$ is the coordinate of the coupling interface, $x < x_C$ and $x > x_C$ are covered by the LB and DV models, respectively (Fig. 2). As before, only the positive velocities $\xi_j > 0$ are described. Negative velocities $\xi_j < 0$ are treated in the same manner due to symmetric coupling based on the unified DV representation in the velocity space. In order to use (27) for calculating $f_{1/2}^{n+1/2}(\boldsymbol{\xi}_{\text{DV},j})$ and $f_{3/2}^{n+1/2}(\boldsymbol{\xi}_{\text{DV},j})$, the VDF should be mapped from LB to DV model in the ghost cells $m = -1$ and $m = 0$. Conversely, $f_{M+1}^n(\boldsymbol{\xi}_{\text{LB},j})$ is reconstructed from $f_1^n(\boldsymbol{\xi}_{\text{DV},j})$ and substituted in (27) to obtain $f_{M+1/2}^{n+1/2}(\boldsymbol{\xi}_{\text{LB},j})$.

The proposed Hermite-based mapping method preserves all the conservation properties because all moments required for the equilibrium function are calculated precisely. However, the FV scheme deals separately with velocities directed in the opposite half-spaces with respect to the coupling interface. For this reason, mass, momentum, and energy fluxes across the coupling interface depend on quadrature rule and, therefore, are not exactly equal for the LB and DV models. In the present study, the polynomial correction (like in [64]) of the flux through the coupling interface is employed to recover the conservation properties. Specifically, edge values $f_{1/2}^{n+1/2}(\boldsymbol{\xi}_{\text{DV},j})$ are replaced by the corrected ones

$$\tilde{f}_{1/2}^{n+1/2}(\boldsymbol{\xi}_{\text{DV},j}) = f_{1/2}^{n+1/2}(\boldsymbol{\xi}_{\text{DV},j})(1 + \mathbf{m}_C \cdot \boldsymbol{\psi}_{\text{DV},j}) \quad (\xi_{\text{DV},j} > 0), \quad (35)$$

where $\boldsymbol{\psi}_j$ is defined in (11) and \mathbf{m}_C is found from

$$\sum_{j=1}^{N_{\text{DV}}} \xi_{\text{DV},j} \boldsymbol{\psi}_{\text{DV},j} \tilde{f}_{\text{DV},j}^{n+1/2} = \sum_{j=1}^{N_{\text{LB}}} \xi_{\text{LB},j} \boldsymbol{\psi}_{\text{LB},j} f_{\text{LB},j}^{n+1/2}. \quad (36)$$

For negative velocities ($\xi_{\text{DV},j} < 0$), the DV solution remains unchanged as well as the LB one. In practice, each component of $\mathbf{m}_C \in \mathbb{R}^5$ is significantly less than unity; therefore, the positivity is also preserved.

5.4. Mesh refinement

The diffuse-reflection boundary condition introduces several singularities into the VDF both in the velocity space and in the physical one. First, the discontinuity exists along the plane $\boldsymbol{\xi} \cdot \mathbf{n} = 0$ and directly on the boundary surface ($\mathbf{x} = \mathbf{x}_B$). For a convex domain, this discontinuity does not enter the gas region [65, 66], since characteristics do not enter into the gas region. Nevertheless, sharp variations of the solution near $\boldsymbol{\xi} \cdot \mathbf{n} = 0$ requires a strong mesh refinement in order to achieve a high-accuracy approximation. Moreover, it is necessary to resolve the logarithmic singularity of the form [67]

$$\frac{\partial f}{\partial \boldsymbol{\xi}} \cdot \mathbf{n} = C_1 \log \boldsymbol{\xi} \cdot \mathbf{n} + O(1), \quad (\boldsymbol{\xi} \cdot \mathbf{n} < 0, \quad \mathbf{x} = \mathbf{x}_B). \quad (37)$$

Second, another logarithmic singularity arises in the physical space along \mathbf{n} [68]:

$$\frac{\partial f}{\partial \mathbf{x}} \cdot \mathbf{n} = \frac{C_2}{k} \log \frac{(\mathbf{x} - \mathbf{x}_B) \cdot \mathbf{n}}{k} + O(1). \quad (38)$$

Here, C_1 and C_2 are some positive constants. It is seen from (38) that the logarithmic singularity of the VDF — and all macroscopic variables as well — takes place for all Knudsen numbers; however, for small k , it becomes highly localized in the Knudsen layer. Therefore, the physical mesh should be refined exponentially as \mathbf{x} goes to \mathbf{x}_B .

6. Results and discussion

6.1. Couette-flow problem

The proposed numerical method is tested for the plane Couette-flow problem, where a gas is embraced between the two parallel plates with non-zero relative velocity. The hybrid approach assumes that a highly

nonequilibrium gas in the Knudsen layer is described using the BGK equation, while the LB model is employed for the internal zone. All the presented results can be reproduced using python code [69].

For the BGK model of the Boltzmann equation, the plane Couette-flow problem can be reduced to the one-dimensional Fredholm integral equation with a weakly singular kernel (see Appendix B for details), which has been solved accurately in [70] and, especially, in [71]. Due to the lack of data on longitudinal heat flux in the mentioned works, we have re-implemented [72] the adaptive collocation method based on the generalized Gauss quadratures presented in [71] for computing the benchmark solutions.

Let the plates be placed at $y = \pm 1/2$ with constant temperature $T = 1$ and velocities $(\pm \Delta v/2, 0, 0)$, where $\Delta v = 0.02$, which is small enough to consider the Couette-flow problem as linear. A completely diffuse reflection is assumed at the plates. The average density is equal to unity: $\int_{-1/2}^{1/2} \rho dy = 1$. The physical space $0 < y < 1/2$ is divided in two subdomains: $0 < y < y_I$ and $y_I < y < 1/2$. The first one consists of identical cells, while the nonuniform mesh in the second one refines as a geometrical sequence near $y = 1/2$. The total number of cells depends on k and varies from 28 to 35.

The VDF in the velocity space varies from the discontinuous sum of two half-Maxwellians at the boundary with complete diffuse-reflection condition to the near-equilibrium form in the vicinity of $y = 0$. Such diversity can be efficiently approximated under the fixed DV set by employing a significantly nonuniform velocity grid with local refinement near $\xi_y = 0$ [73, 74, 75]. In the present paper, the nonuniform Cartesian lattice is cut off by the sphere of radius $\xi^{(\text{cut})} = 4$. Along ξ_x and ξ_z axis, the nodes are distributed as the scaled roots of the Hermite polynomials:

$$\xi_{\alpha,j} = x_{\mathcal{H}j}R, \quad w_{\alpha,j} = w_{\mathcal{H}j} \exp(x_{\mathcal{H}j}^2)R, \quad R = 2\xi^{(\text{cut})} \left(\sum_{i=1}^{2N_\alpha} w_{\mathcal{H}i} \exp(x_{\mathcal{H}i}^2) \right)^{-1}, \quad j = 1, \dots, 2N_\alpha, \quad (39)$$

where $x_{\mathcal{H}j}$ and $w_{\mathcal{H}j}$ are nodes and weights of the $(2N_\alpha)$ -point Gauss–Hermite quadrature. Along $\xi_y > 0$ semiaxis, the nodes are distributed as a polynomial (particularly, quadratic $p = 2$) sequence:

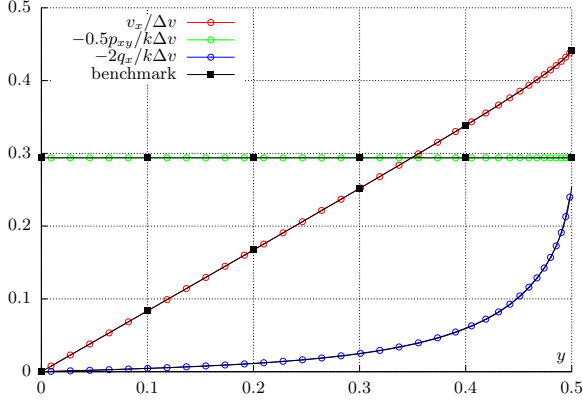
$$\xi_{y,j} = \sum_{i=0}^{j-1} \frac{w_{y,i} + w_{y,i+1}}{2}, \quad w_{y,j} = w_{y,1} + (j-1)^p \left(\xi^{(\text{cut})} - N_y w_{y,1} \right) \left(\sum_{i=0}^{N_y-1} i^p \right)^{-1}, \quad j = 1, \dots, N_y, \quad (40)$$

where $w_{y,0} = 0$, $w_{y,1} = 0.1$ is the minimal width of the cell in the velocity space. The quadrature weight in \mathbb{R}^3 of discrete velocity ξ_j is equal to $\prod_\alpha w_{\alpha,j}$. For all the presented DVM solutions, $N_{x/z} = 8$ and $N_y = 16$ are chosen. The discrete velocities with $|\xi_j| > \xi^{(\text{cut})}$ are excluded from the velocity grid; therefore, the total number of discrete velocities $N_{\text{DV}} = 5928$.

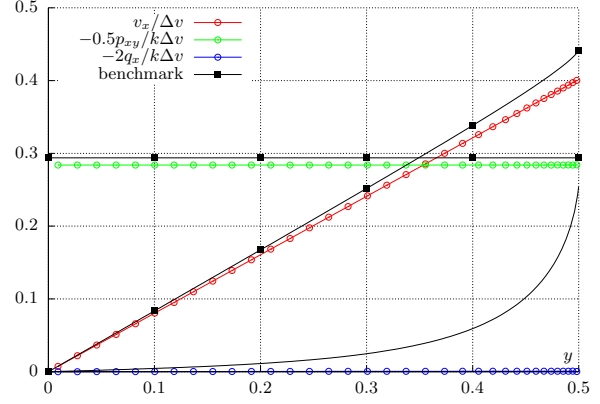
Here it is important to mention that the longitudinal heat flux q_x exists in the linear Couette-flow problem, or to be exact, in the Knudsen layer only and, therefore, decays exponentially with the distance from the boundary [42]. This heat flux is caused by the diffuse-reflection boundary condition and has non-polar singularity on k at the boundary. Hence, it cannot be reproduced by the Navier–Stokes or any other high-order fluid-dynamic-type equations obtained from the Hilbert or Chapman–Enskog expansions. The same conclusion holds for the classical LB models.

6.2. Numerical analysis

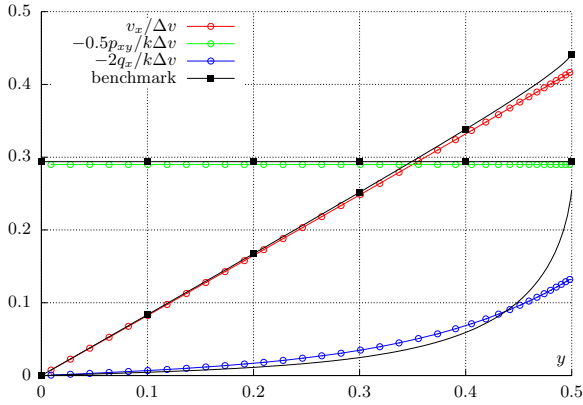
The numerical results obtained by the pure DV and LB methods for $k = 0.1$ are shown in Fig. 3. The nonuniform velocity grid refined at the sharp variations of the VDF yields a small discrepancy between the DV and benchmark profiles (Fig. 3a). As for the LB method, the 5-order D3Q19 model and 7-order D3Q39 model [20] based on the Gauss–Hermite quadratures are considered, along with special 7-order D3Q96 model developed for the boundary-value problems driven by the diffuse-reflection boundary condition [23]. Ability to capture rarefied-gas effects arising from the kinetic boundary conditions is observed from the profile of the longitudinal heat flux q_x . In particular, models of the Navier–Stokes level do not capture it due to lack of additional degrees of freedom, e.g., the D3Q19 model does not cover the third-order moments of the VDF (Fig. 3b). Instead, there is a small spurious positive heat flux in Fig. 3b, which is $O(\Delta v^3)$ and closely



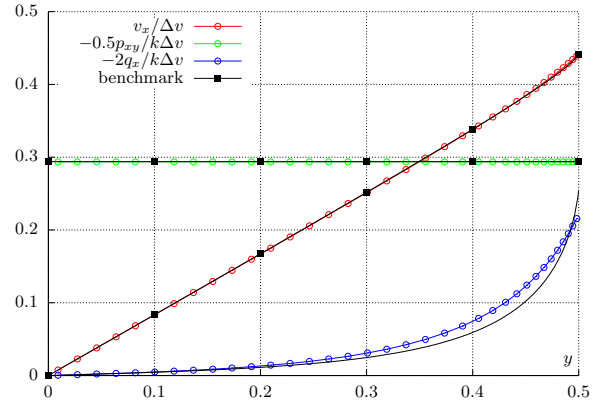
(a) DV method



(b) LB method: D3Q19

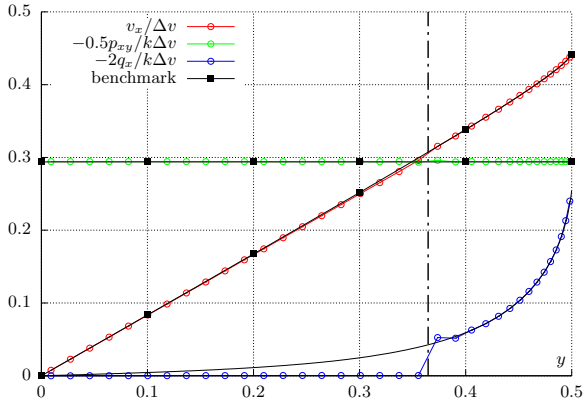


(c) LB method: D3Q39

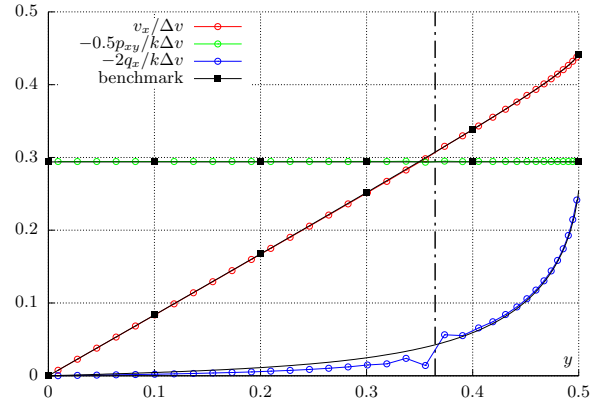


(d) LB method: D3Q96

Figure 3: Numerical solution of the Couette-flow problem for $k = 0.1$ obtained by pure DV or LB methods. The black lines are the high-accuracy solution for the BGK model. The black boxes correspond to the tabulated solutions [71].

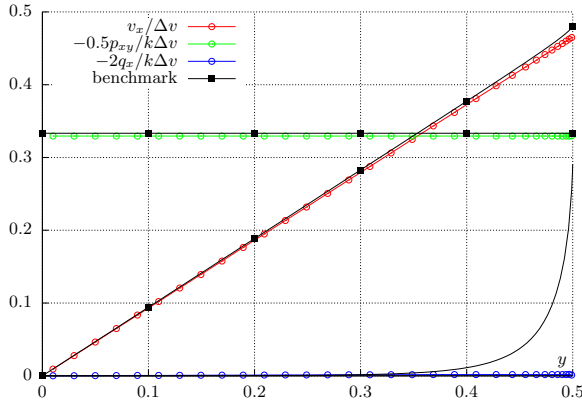


(a) hybrid: DV and D3Q19

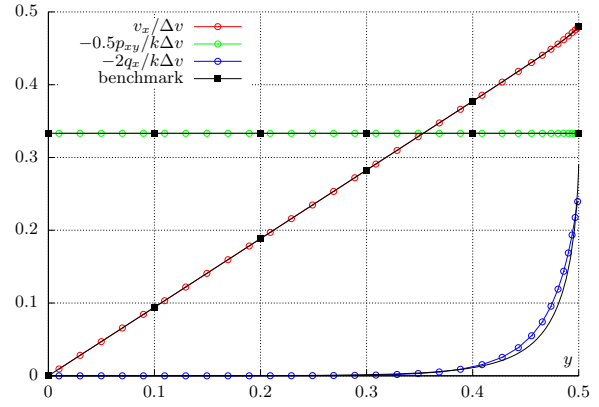


(b) hybrid: DV and D3Q96

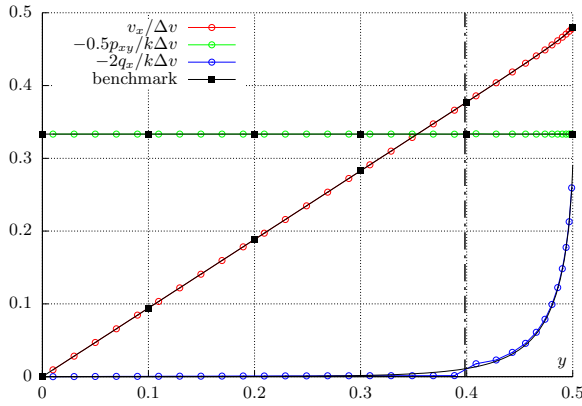
Figure 4: Numerical solution of the Couette-flow problem for $k = 0.1$ obtained by the proposed hybrid method. There are 1.2 mean free paths between the boundary and coupling interface marked with the dash-dotted line. The black lines are the high-accuracy benchmark solution. The black boxes correspond to the tabulated values from [71].



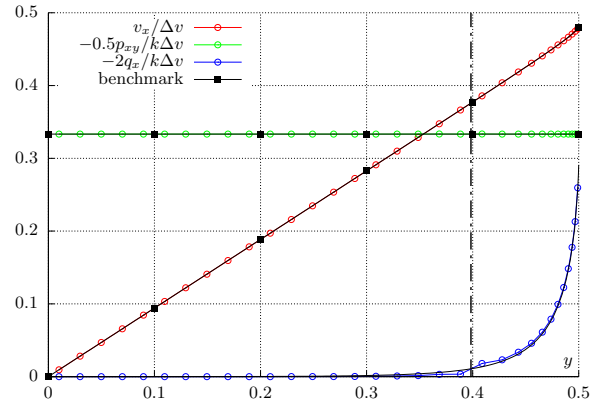
(a) LB method: D3Q19



(b) LB method: D3Q96

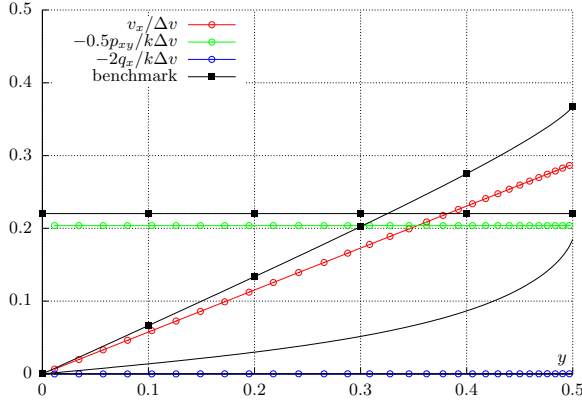


(c) hybrid: DV and D3Q19

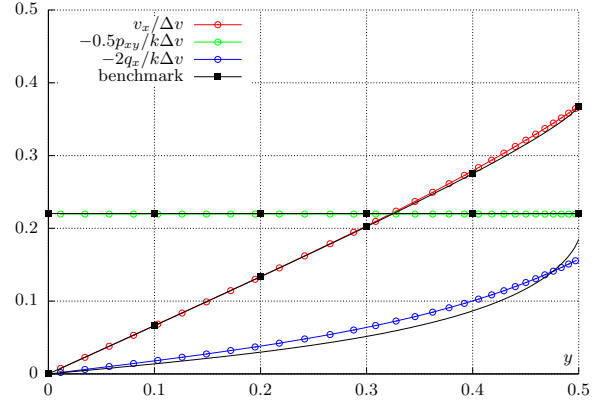


(d) hybrid: DV and D3Q96

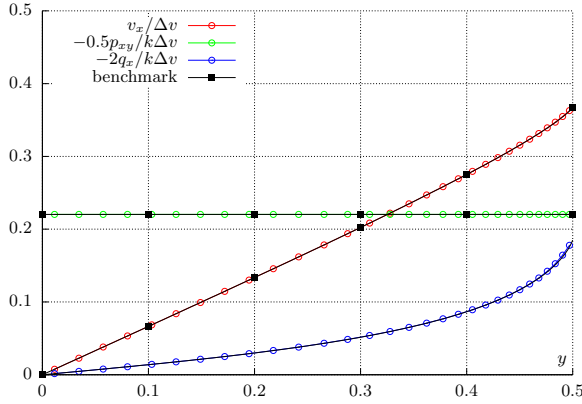
Figure 5: Numerical solution of the Couette-flow problem for $k = 0.03$ obtained by the proposed hybrid method. There are 3 mean free paths between the boundary and coupling interface marked with the dash-dotted line. The black lines are the high-accuracy benchmark solution. The black boxes correspond to the tabulated values from [71].



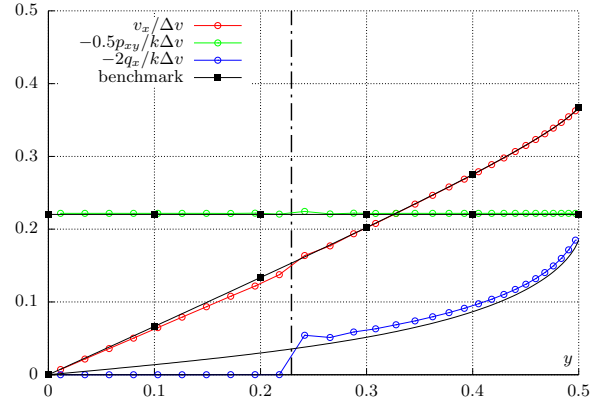
(a) LB method: D3Q19



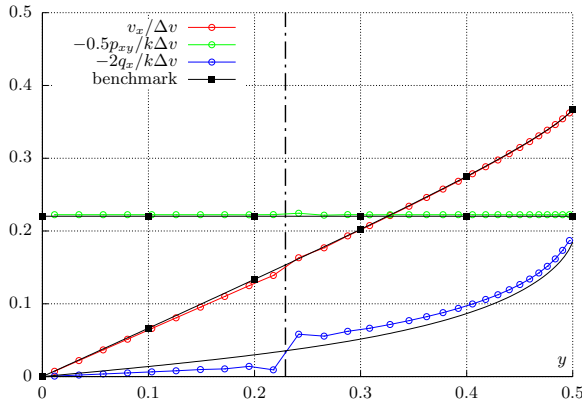
(b) LB method: D3Q96



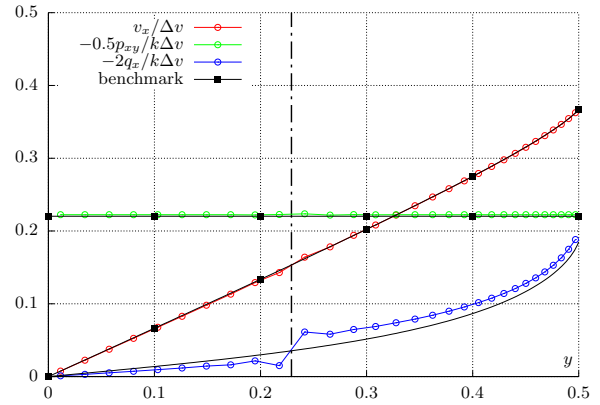
(c) DV method



(d) hybrid: DV and D3Q19



(e) hybrid: DV and D3Q39



(f) hybrid: DV and D3Q96

Figure 6: Numerical solution of the Couette-flow problem for $k = 0.3$ obtained by the proposed hybrid method. There are 0.8 mean free paths between the boundary and coupling interface marked with the dash-dotted line. The black lines are the high-accuracy benchmark solution. The black boxes correspond to the tabulated values from [71].

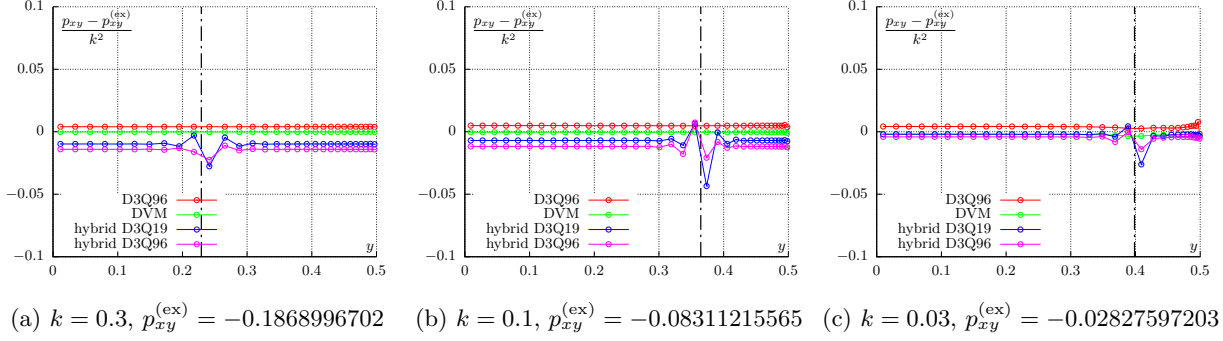


Figure 7: Absolute numerical error of the shear stress obtained by the pure and hybrid schemes. The dash-dotted lines correspond to the coupling interface used for the domain decomposition. The reference values $p_{xy}^{(ex)}$ are taken from [71].

associated with the stress tensor and velocity. The model D3Q39 partially reproduces the heat flux (Fig. 3c), while the D3Q96 q_x profile appears to be quite close to the exact one (Fig. 3d).

Increasing the order of the LB model helps to capture the corresponding low-order moments of the VDF but failed to describe its high-order relaxation correctly. However, the LB models augmented by special velocity groups are capable of reproducing the Knudsen layer to some extent. The augmented model D3Q96 reproduces the Maxwell half-range (or wall) moments better than D3Q39, which results in better reproduction of the diffuse-reflection boundary condition. As a result, D3Q96 produces qualitatively correct results for the longitudinal heat flux, which has non-thermo-hydrodynamical nature, although it does not recover thermo-hydrodynamics.

The numerical results for the hybrid schemes are shown in Fig. 4. Quantities v_x and p_{xy} are close to the exact solution, but there is a noticeable distortion behind the coupling interface in the D3Q19 velocity profile. Hybrid q_x is close to the pure DV one only in the kinetic region (the DV part of the hybrid solution). There are small oscillations of macroscopic variables in the buffer zone, and they are particularly noticeable for q_x , since its profile is multiplied by factor 40. The amplitude of these oscillations is proportional to the high-order terms of the Hermite expansion of the VDF that are not included in the employed mapping method. These terms decrease exponentially as the coupling interface moves away from $y = 1/2$. The numerical results for $k = 0.03$ shown in Fig. 5, where 3 mean free paths (in contrast to 1.2 for $k = 0.1$) are covered by DV method, clearly illustrate this fact.

For larger k , the advantage of the DV method over the LB one in terms of accuracy becomes more evident, since rarefied-gas effects amplify considerably (Fig. 6). The D3Q19 model loses its accuracy most of all: there is a substantial deviation from the benchmark profiles of p_{xy} and v_x in Fig. 6a. Although D3Q96 can reproduce half-range (wall) moments most accurately within the given order, it fails to reproduce the complex structure of a highly nonequilibrium VDF with sharp variations around plane $\xi_y = 0$ (Fig. 6b). In contrast, the DV method with the velocity grid refined near $\xi_y = 0$ adequately copes with this task. One cannot conclude the same for the results obtained by hybrid schemes. There is a noticeable discrepancy for q_x and a kink for v_x in Fig. 6d–f. The proximity of the coupling interface to the boundary in terms of mean free path is the primary reason for the observed lack of accuracy. Note also that the hybrid method based on the D3Q96 model has a minimal kinking of the velocity profile in comparison to D3Q19 and D3Q39.

The shear stress profiles look constant in Figs. 4, 5, and 6, since the absolute error is everywhere smaller than $0.06k^2$, which is easily seen in Fig. 7. The largest error is observed in the points in the vicinity of the coupling interface. In the absence of conservative correction of fluxes on the coupling interface (35), these oscillations turn into monotonic jumps, which introduce much more error into results. This fact clearly confirms the well-known importance of preserving the conservation properties by a numerical method. Incidentally, let us note that the obtained numerical accuracy is sufficient to distinguish molecular potentials [76, 77].

Finally, let us touch upon the efficiency of the proposed hybrid scheme. The computational speed-up with respect to the pure DV scheme is shown in Fig. 8 as a ratio of the corresponding CPU times, while the

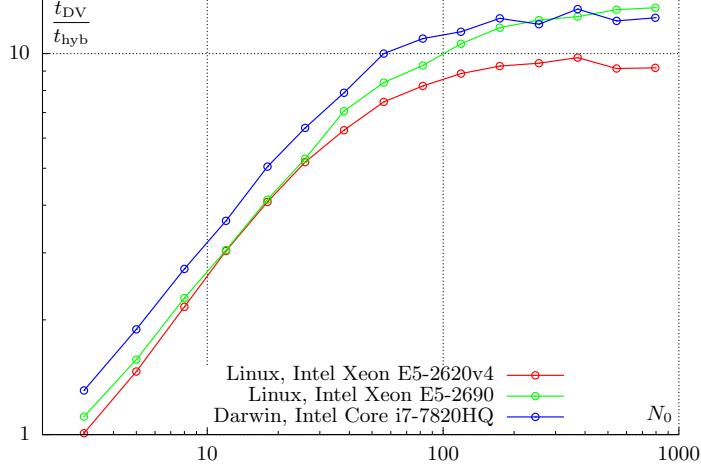


Figure 8: Computational speed-up yielded by the hybrid method for different CPUs and operational systems. N_0 is the number of cells in the kinetic zone, $10N_0$ is the number of cells in the bulk region, t_{DV} and t_{hyb} are the total CPU times elapsed by the DV and hybrid methods, respectively.

ratio of cells in the kinetic and bulk regions remains constant. One can see that the efficiency of the hybrid method achieves the optimum value when the number of cells in the kinetic region is more than 10^2 . Note that the asymptotic speed-up can be slightly higher than the optimum one (12–13 versus 11 in Fig. 8). It is mainly due to memory saving, which results in fewer cache misses.

6.3. Breakdown criterion

A multiscale hybrid method based on the domain decomposition procedure should be supplied with the so-called equilibrium breakdown criterion, which determines the position of the coupling interface between different models for approximation of the VDF. The typical way to quantify this criterion is to introduce an appropriate equilibrium breakdown parameter E and compare it with some predefined value ϵ_E . The DV method is used only in nonequilibrium regions, specifically in cells, where $E > \epsilon_E$, while the LB method is employed in the others.

Longitudinal heat flux q_x appears only in the Knudsen layer and, therefore, can serve as an equilibrium breakdown parameter for the investigated Couette-flow problem, but not in the general case. Criteria based on deviation of the VDF from the truncated Chapman–Enskog expansion is natural for kinetic schemes. For instance, quantities $E_p = \|f - f^{(NSF)}\|_p / \|f\|_p$, the deviation from the Navier–Stokes–Fourier (NSF) order of approximation [78]:

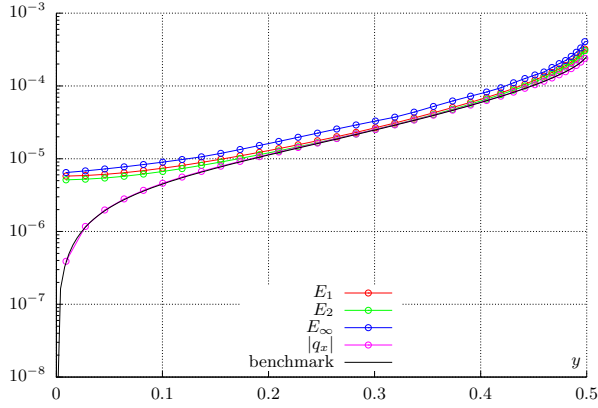
$$f_{DV,j}^{(NSF)} = f_{DV,j}^{(eq)} \left(1 + \frac{c_{\alpha,j} c_{\beta,j} P_{\alpha\beta}}{2pT} + \frac{c_{\alpha,j} q_\alpha}{pT} \left(\frac{c_j^2}{5T} - 1 \right) \right), \quad (41)$$

$$f_{LB,j}^{(NSF)} = f_{LB,j}^{(eq)} + w_j \xi_{\alpha,j} \left(P_{\alpha\beta} (\xi_{\beta,j} (1 + \xi_{\gamma,j} v_\gamma) - 2v_\beta) + q_\alpha \left(\frac{\xi_j^2}{5} - 1 \right) \right), \quad (42)$$

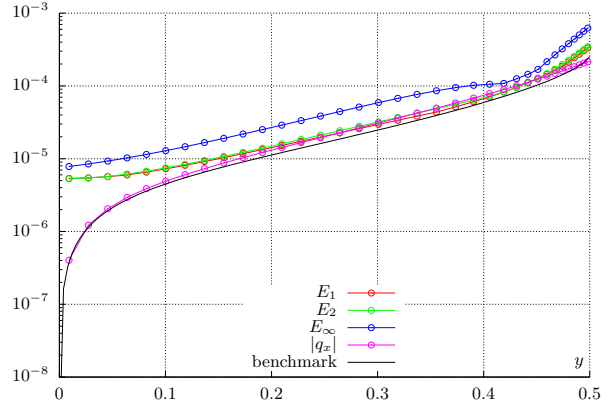
where $P_{\alpha\beta} = p_{\alpha\beta} - \rho T \delta_{\alpha\beta}$ and $c_{\alpha,j} = \xi_{\alpha,j} - v_\alpha$, are shown in Fig. 9 for the following norms in the discrete velocity space:

$$\|f\|_p = \left(\sum_j |f_j|^p \right)^{1/p}, \quad p = 1, 2, \quad \|f\|_\infty = \max_j |f_j|. \quad (43)$$

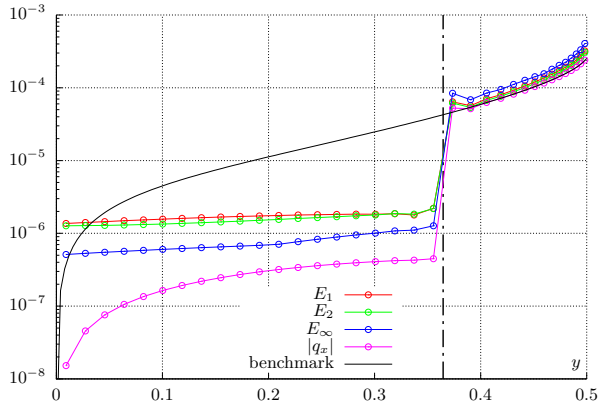
The D3Q19 model produces an almost constant profile (Fig. 9c) since it describes nothing beyond the NSF level. The D3Q96 profile (Fig. 9b) is close to the DV one (Fig. 9a), which indirectly indicates that



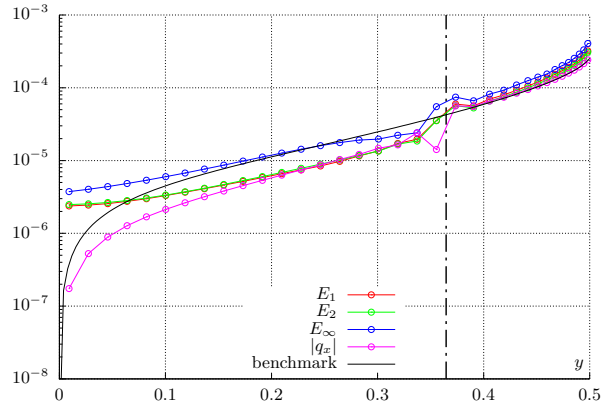
(a) DV method



(b) LB method: D3Q96



(c) hybrid: DV and D3Q19



(d) hybrid: DV and D3Q96

Figure 9: Quantities that can serve as a equilibrium breakdown parameter for $k = 0.1$.

this LB model gives an acceptable approximation for the Couette-flow problem. Due to the diffuse-reflection boundary condition, there is a discontinuity of the VDF on the boundary, which decays monotonically and faster than any inverse power of distance from the boundary. Therefore, all the breakdown parameters reach their maximum on the boundary; however, E_∞ relaxes in a non-smooth way. It is probably due to crude approximation of the sharp variations of the VDF in the Knudsen layer. For the D3Q96 model, E_∞ noticeably exceeds $E_{1,2}$ (Fig. 9b), which can be explained by its peculiar properties minimizing the wall moment errors. The Hermite-based coupling induces oscillations (Fig. 9c, 9d) since it is unable to reconstruct nonequilibrium part of the VDF. The sharp drop in Fig. 9c indicates that the coupling interface is too close to the boundary, while the smoother transition in Fig. 9d can be considered as more acceptable. Nevertheless, both hybrid schemes have almost the same DV part of the solution.

7. Conclusions and perspectives

In this paper, we have presented a new algorithm for coupling the LB and DV methods for solving the Boltzmann kinetic equation. The Couette flow of a rarefied BGK gas has been analyzed numerically as a test example. The continuum gas behavior is described by several Gauss–Hermite LB models with various numbers of discrete velocities ranging from 19 to 96. Incorporating the augmented [23] LB models positively affects the solution accuracy in comparison to the conventional LB models. The Knudsen layer is captured accurately by the DV method with highly nonuniform velocity grids. The numerical stress-tensor anisotropy generated by such grids is eliminated by minimizing the 7-moment discrete entropy functional. The physical mesh refinement near the boundary allows to effectively approximate the weak singularity of the profiles of the macroscopic variables. The LB and DV solutions are matched by means of projection onto the truncated Hermite basis. The second-order FV solution of both subdomains are supplied by two ghost cells with the reconstructed values. The additional polynomial correction procedure of the interfacial DV flux has been employed to ensure conservative properties of the coupling algorithm.

Since the employed LB models are suited for the isothermal hydrodynamics, the proposed hybrid method is applicable to flows with Mach number $\lesssim 0.3$. The subsonic regime is quite challenging for the DSMC-based methods due to the inherent stochastic noise, but the deterministic approaches work well.

The other LB models (e.g., for supersonic flows, compressible, and thermal flows [79, 80, 81]) can be potentially incorporated into the hybrid method. The entropic models [53, 54, 55] are promising due to their enhanced stability for low viscosities (large Reynolds numbers). Using of the regularized high-order LB models [58, 27, 59] for the hybrid schemes is interested as well. One can conclude that the improvements in employed LB model should be directed to the better reproduction of the higher Maxwell moments and half-range (wall) moments [25]. In this case, the mapping method should also be upgraded by involving higher-order and wall moments.

Adaptive coupling of the LB and DV methods under the unified FV formulation can be considered as a variant of the DV methodologies based on adaptive grids in velocity space [82, 83, 84]. The adaptation of the DV set according to the local flow regime provides room for improving the efficiency of numerical methods and can serve as a foundation of hybrid schemes for multiscale compressible flows.

Acknowledgements

This work was supported by the Russian Foundation for Basic Research (Grants 18-01-00899, 18-07-01500). The authors are grateful to the referees for many constructive comments that helped in improving the quality of the paper.

Appendix A. Third-order TVD limiter for the FV scheme

Let us approximate the one-dimensional transport equation $\partial f/\partial t + \xi\partial f/\partial x$ in the FV manner with constant mesh (Δx) and time (Δt) steps:

$$f_m^{n+1} = f_m^n - \gamma \left(f_{m+1/2}^{n+1/2} - f_{m-1/2}^{n+1/2} \right), \quad \gamma = \frac{\xi \Delta t}{\Delta x} \geq 0, \quad m = 1, \dots, M, \quad n \in \mathbb{N}, \quad (\text{A.1})$$

where the reconstructed edge values for the third-point stencil are written in the following form:

$$f_{m+1/2}^{n+1/2} = f_m^n + \frac{1-\gamma}{2} \phi\left(\frac{\Delta_-}{\Delta_+}\right) \Delta_+, \quad m = 1, \dots, M, \quad (\text{A.2})$$

where $\Delta_{\pm} = \pm(f_{m\pm 1}^n - f_m^n)$, function $\phi(\theta)$ is usually called a flux limiter. Within the one-point stencil for positive velocities $\xi_j > 0$, it is possible to construct the first-order (upwind) scheme only ($\phi = 0$). The second-order accuracy can be achieved, if $\phi(1+x) = 1 + O(x)$. For the third-order accuracy, the following condition is sufficient:

$$\phi(1+x) = 1 + \frac{1+\gamma}{3}x + O(x^2). \quad (\text{A.3})$$

Taking into account the CFL condition $\gamma \leq 1$ and non-negativity of the limiter for monotonic functions $\phi(\theta \geq 0) \geq 0$, one can obtain the following sufficient conditions for the TVD property of the numerical scheme:

$$\begin{cases} \phi(\theta) = 0, & \theta < 0, \\ \phi(\theta) \leq \frac{2}{\gamma}\theta, & \theta \geq 0, \\ 0 \leq \phi(\theta) \leq \frac{2}{1-\gamma}. \end{cases} \quad (\text{A.4})$$

Combining (A.3) and (A.4), one can construct a third-order TVD limiter:

$$\phi(\theta) = \begin{cases} 0, & \theta < 0, \\ \min\left(\frac{2}{\gamma}\theta, \frac{1+\gamma}{3}\theta + \frac{2-\gamma}{3}, \frac{2}{1-\gamma}\right), & \theta \geq 0, \end{cases} \quad (\text{A.5})$$

which is used in the present study, but for nonuniform mesh step (28). Let us note that inequalities (A.4) are often replaced by stronger ones, independent of γ , especially when nonlinear transport equation is considered.

Appendix B. Solution of the linear Couette-flow problem for the BGK model

For symmetry reasons, the steady-state behavior of the gas in the Couette flow at $\Delta v \rightarrow 0$ and arbitrary k is described by the following VDF:

$$f(\boldsymbol{\xi}) = \omega(\boldsymbol{\xi})(1 + \Delta v \xi_x \Phi(y, \xi_y, \xi)), \quad \xi = |\boldsymbol{\xi}|, \quad (\text{B.1})$$

where $\omega(\boldsymbol{\xi})$ is defined in (19) and Φ is governed by

$$\tau \xi_y \frac{\partial \Phi}{\partial y} = \frac{v_x}{\Delta v} - \Phi, \quad \Phi\left(y = \mp \frac{1}{2}, \xi_y \geq 0, \xi\right) = \mp \frac{1}{2}, \quad (\text{B.2})$$

which is derived under the assumption of the BGK model of collisional term [42]. The macroscopic variables are the following moments of Φ :

$$v_x = \Delta v \int \xi_x^2 \Phi \omega d\xi, \quad p_{xy} = \Delta v \int \xi_x^2 \xi_y \Phi \omega d\xi, \quad q_x = \frac{\Delta v}{2} \int \xi_x^2 \xi^2 \Phi \omega d\xi - \frac{5}{2} v_x. \quad (\text{B.3})$$

The solution of (B.2) can be represented as

$$\Phi\left(|y| \leq \frac{1}{2}, \xi_y \geq 0, \xi\right) = \mp \frac{1}{2} \exp\left(\mp \frac{1 \pm 2y}{2\tau \xi_y}\right) + \frac{1}{2\tau \xi_y} \int_{\mp \frac{1}{2}}^y \exp\left(-\frac{y-s}{\tau \xi_y}\right) g(s) ds, \quad (\text{B.4})$$

where $g(y) = 2v_x/\Delta v$ is obtained from the following integral equation [85]:

$$\sqrt{\pi} g(y) = \mathcal{J}_0\left(\frac{1-2y}{2k}\right) - \mathcal{J}_0\left(\frac{1+2y}{2k}\right) + \frac{1}{k} \int_0^{\frac{1}{2}} \left[\mathcal{J}_{-1}\left(\frac{|y-s|}{k}\right) - \mathcal{J}_{-1}\left(\frac{y+s}{k}\right) \right] g(s) ds. \quad (\text{B.5})$$

Here, $\mathcal{J}_n(s)$ are the Abramowitz functions [86]:

$$\mathcal{J}_n(s) = \int_0^\infty t^n \exp\left(-t^2 - \frac{s}{t}\right) dt, \quad s \geq 0, \quad n \in \mathbb{Z}. \quad (\text{B.6})$$

The remaining macroscopic variables are calculated as follows:

$$\frac{p_{xy}}{\Delta v} = -\frac{\tau}{\sqrt{\pi}} \left(\mathcal{J}_2(0) - \mathcal{J}_2\left(\frac{1}{k}\right) + \frac{1}{k} \int_0^{\frac{1}{2}} \left[\mathcal{J}_1\left(\frac{1-2s}{2k}\right) - \mathcal{J}_1\left(\frac{1+2s}{2k}\right) \right] g(s) ds \right), \quad (\text{B.7})$$

$$\begin{aligned} \frac{q_x}{\Delta v} = & \frac{1}{2\sqrt{\pi}} \left(\mathcal{J}_2\left(\frac{1-2y}{2k}\right) - \mathcal{J}_2\left(\frac{1+2y}{2k}\right) \right) \\ & + \frac{1}{k} \int_0^{\frac{1}{2}} \left[\mathcal{J}_1\left(\frac{|y-s|}{k}\right) - \mathcal{J}_1\left(\frac{y+s}{k}\right) \right] g(s) ds - \frac{g(y)}{4}. \end{aligned} \quad (\text{B.8})$$

Methods of a high-accuracy solution of (B.5) are presented in [70, 71].

References

- [1] G. Dimarco, L. Pareschi, Numerical methods for kinetic equations, *Acta Numer.* 23 (2014) 369–520. doi:10.1017/S0962492914000063.
- [2] J.-F. Bourgat, P. Le Tallec, M. Tidriri, Coupling boltzmann and navier–stokes equations by friction, *J. Comput. Phys.* 127 (2) (1996) 227–245. doi:10.1006/jcph.1996.0172.
- [3] P. Le Tallec, F. Mallinger, Coupling boltzmann and navier–stokes equations by half fluxes, *J. Comput. Phys.* 136 (1) (1997) 51–67. doi:10.1006/jcph.1997.5729.
- [4] V. V. Potkin, Kinetic analysis of difference schemes for gas dynamics, *USSR Comp. Math. Math. Phys.* 15 (6) (1975) 126–132. doi:10.1016/0041-5553(75)90208-6.
- [5] D. I. Pullin, Direct simulation methods for compressible inviscid ideal-gas flow, *J. Comput. Phys.* 34 (2) (1980) 231–244. doi:10.1016/0021-9991(80)90107-2.
- [6] R. D. Reitz, One-dimensional compressible gas dynamics calculations using the boltzmann equation, *J. Comput. Phys.* 42 (1) (1981) 108–123. doi:10.1016/0021-9991(81)90235-7.
- [7] V. V. Aristov, F. G. Cheremisin, A solution to euler and navier-stokes equations based on the operator splitting of a kinetic equation, *Dokl. Akad. Nauk SSSR+* 272 (3) (1983) 555–559.
- [8] T. G. Elizarova, B. N. Chetverushkin, Kinetic algorithms for calculating gas dynamic flows, *USSR Comp. Math. Math. Phys.* 25 (5) (1985) 164–169. doi:10.1016/0041-5553(85)90194-6.
- [9] S. M. Deshpande, Kinetic theory based new upwind methods for inviscid compressible flows, in: 24th Aerospace Sciences Meeting, 1986, p. 275. doi:10.2514/6.1986-275.
- [10] K. H. Prendergast, K. Xu, Numerical hydrodynamics from gas-kinetic theory, *J. Comput. Phys.* 109 (1) (1993) 53–66. doi:10.1006/jcph.1993.1198.
- [11] S.-Y. Chou, D. Baganoff, Kinetic flux–vector splitting for the navier–stokes equations, *J. Comput. Phys.* 130 (2) (1997) 217–230. doi:10.1006/jcph.1996.5579.
- [12] T. Ohwada, K. Xu, The kinetic scheme for the full-burnett equations, *J. Comput. Phys.* 201 (1) (2004) 315–332. doi:10.1016/j.jcp.2004.05.017.

- [13] T. Ohwada, S. Kobayashi, Management of discontinuous reconstruction in kinetic schemes, *J. Comput. Phys.* 197 (1) (2004) 116–138. doi:10.1016/j.jcp.2003.11.020.
- [14] T. Ohwada, S. Fukata, Simple derivation of high-resolution schemes for compressible flows by kinetic approach, *J. Comput. Phys.* 211 (2) (2006) 424–447. doi:10.1016/j.jcp.2005.04.026.
- [15] U. Frisch, B. Hasslacher, Y. Pomeau, Lattice-gas automata for the navier-stokes equation, *Phys. Rev. Lett.* 56 (14) (1986) 1505. doi:10.1103/PhysRevLett.56.1505.
- [16] Y. H. Qian, D. d’Humières, P. Lallemand, Lattice bgk models for navier-stokes equation, *Europhys. Lett.* 17 (6) (1992) 479–484. doi:10.1209/0295-5075/17/6/001.
- [17] F. Higuera, S. Succi, R. Benzi, Lattice gas dynamics with enhanced collisions, *Europhys. Lett.* 9 (1989) 345–349. doi:10.1209/0295-5075/9/4/008.
- [18] R. Benzi, S. Succi, M. Vergassola, The lattice boltzmann equation: theory and applications, *Phys. Rep.* 222 (1992) 145–197. doi:doi:10.1016/0370-1573(92)90090-m.
- [19] S. Succi, *The lattice Boltzmann equation: for fluid dynamics and beyond*, Oxford university press, 2001.
- [20] X. Shan, X.-F. Yuan, H. Chen, Kinetic theory representation of hydrodynamics: a way beyond the navier–stokes equation, *J. Fluid Mech.* 550 (2006) 413–441. doi:10.1017/S0022112005008153.
- [21] Y. Gan, A. Xu, G. Zhang, Y. Zhang, S. Succi, Discrete boltzmann trans-scale modeling of high-speed compressible flows, *Phys. Rev. E* 95 (2018) 053312. doi:10.1103/PhysRevE.97.053312.
- [22] Y. Zhang, A. Xu, G. Zhang, Y. Gan, Z. Chen, S. Succi, Entropy production in thermal phase separation: a kinetic-theory approach, *Soft Matter* 15 (2019) 2245–2259. doi:10.1039/C8SM02637H.
- [23] C. Feuchter, W. Schleifenbaum, High-order lattice boltzmann models for wall-bounded flows at finite knudsen numbers, *Phys. Rev. E* 94 (1) (2016) 013304. doi:10.1103/PhysRevE.94.013304.
- [24] V. Ambrus, V. Sofonea, Implementation of diffuse-reflection boundary conditions using lattice boltzmann models based on half-space gauss–laguerre quadratures, *Phys. Rev. E* 89 (2014) 041301(R). doi:10.1103/PhysRevE.96.013311.
- [25] V. Ambrus, V. Sofonea, Lattice boltzmann models based on half-range gauss–hermite quadratures, *J. Comp. Phys.* 316 (2016) 760–768. doi:10.1016/j.jcp.2016.04.010.
- [26] V. E. Ambrus, V. Sofonea, Application of mixed quadrature lattice boltzmann models for the simulation of poiseuille flow at non-negligible values of the knudsen number, *J. Comp. Sci.* 17 (2016) 403–417. doi:10.1016/j.jocs.2016.03.016.
- [27] A. Montessori, P. Prestininzi, M. La Rocca, S. Succi, Lattice boltzmann approach for complex nonequilibrium flows, *Phys. Rev. E* 92 (2015) 043308. doi:10.1103/PhysRevE.92.043308.
- [28] J.-P. Rivet, J. P. Boon, *Lattice gas hydrodynamics*, Cambridge University Press, 2001.
- [29] J. E. Broadwell, Shock structure in a simple discrete velocity gas, *Phys. Fluids* 7 (8) (1964) 1243–1247. doi:10.1063/1.1711368.
- [30] R. Gatignol, *Théorie cinétique des gaz à répartition discrète de vitesses*, Springer verlag, 1975. doi:10.1007/3-540-07156-3.
- [31] J. Meng, Y. Zhang, X. Shan, Multiscale lattice boltzmann approach to modeling gas flows, *Phys. Rev. E* 83 (2011) 046701. doi:10.1103/PhysRevE.83.046701.
- [32] G. Di Staso, H. J. H. Clercx, S. Succi, F. Toschi, DSMC–LBM mapping scheme for rarefied and non-rarefied gas flows, *J. Comp. Sci.* 17 (2016) 357–369. doi:10.1016/j.jocs.2016.04.011.

- [33] G. Di Staso, S. Srivastava, E. Arlemark, H. J. H. Clercx, F. Toschi, Hybrid lattice boltzmann-direct simulation monte carlo approach for flows in three-dimensional geometries, *Comput. Fluids* (2018). doi:10.1016/j.compfluid.2018.03.043.
- [34] S. Succi, Lattice boltzmann beyond navier-stokes: Where do we stand?, in: *AIP Conference Proceedings*, Vol. 1786, AIP Publishing, 2016, p. 030001. doi:10.1063/1.4967538.
- [35] O. Ilyin, A method for simulating the dynamics of rarefied gas based on lattice boltzmann equations and the bgk equation, *Comp. Math. and Math. Phys.* 58 (2018) 1817–1827. doi:10.1134/S0965542518110052.
- [36] V. V. Aristov, O. V. Ilyin, O. A. Rogozin, A hybrid numerical scheme based on coupling discrete-velocities models for the bgk and lbgk equations, in: *AIP Conference Proceedings*, Vol. 2132, AIP Publishing, 2019, p. 060007. doi:10.1063/1.5119547.
- [37] F. Nannelli, S. Succi, The lattice boltzmann equation on irregular lattices, *J. Stat. Phys.* 68 (3-4) (1992) 401–407. doi:10.1007/BF01341755.
- [38] G. Peng, H. Xi, C. Duncan, S.-H. Chou, Finite volume scheme for the lattice boltzmann method on unstructured meshes, *Phys. Rev. E* 59 (4) (1999) 4675. doi:10.1103/PhysRevE.59.4675.
- [39] D. V. Patil, K. Lakshmisha, Finite volume tvd formulation of lattice boltzmann simulation on unstructured mesh, *J. Comput. Phys.* 228 (14) (2009) 5262–5279. doi:10.1016/j.jcp.2009.04.008.
- [40] W. Li, L.-S. Luo, Finite volume lattice boltzmann method for nearly incompressible flows on arbitrary unstructured meshes, *Commun. Comput. Phys.* 20 (2) (2016) 301–324. doi:10.4208/cicp.211015.040316a.
- [41] C. Cercignani, *Rarefied gas dynamics: from basic concepts to actual calculations*, Cambridge University Press, 2000.
- [42] Y. Sone, *Molecular gas dynamics: theory, techniques, and applications*, Birkhäuser, Boston, 2007.
- [43] P. L. Bhatnagar, E. P. Gross, M. Krook, A model for collision processes in gases. i. small amplitude processes in charged and neutral one-component systems, *Phys. Rev.* 94 (1954) 511–525. doi:10.1103/PhysRev.94.511.
- [44] P. Welander, On the temperature jump in a rarefied gas, *Arkiv Fysik* 7 (1954) 507–553.
- [45] H. Cabannes, *The discrete boltzmann equation (theory and applications)*, Lecture notes (1980).
- [46] V. V. Aristov, *Direct methods for solving the Boltzmann equation and study of nonequilibrium flows*, Kluwer Academic Publishers, Dordrecht, 2001.
- [47] L. Mieussens, Discrete velocity model and implicit scheme for the bgk equation of rarefied gas dynamics, *Math. Models Methods Appl. Sci.* 10 (08) (2000) 1121–1149. doi:10.1142/S0218202500000562.
- [48] P. Charrier, B. Dubroca, J. L. Feugeas, Levermore’s moment closure of discrete boltzmann equations for non-equilibrium kinetic flows, in: *21st international symposium on rarefied gas dynamics*, Vol. 1, 1999, pp. 39–40.
- [49] T. Krüger, H. Kusumaatmaja, A. Kuzmin, O. Shardt, G. Silva, E. Viggen, *The Lattice Boltzmann Method. Principles and Practice*, Springer, 2017.
- [50] X. He, L.-S. Luo, A priori derivation of the lattice boltzmann equation, *Phys. Rev. E* 55 (6) (1997) R6333–R6336. doi:10.1103/PhysRevE.55.R6333.

- [51] X. Shan, X. He, Discretization of the velocity space in the solution of the boltzmann equation, *Phys. Rev. Lett.* 80 (1998) 65–68. doi:10.1103/PhysRevLett.80.65.
- [52] X. Shan, General solution of lattices for cartesian lattice bhatanagar–gross–krook models, *Phys. Rev. E* 81 (2010) 036702. doi:10.1103/PhysRevE.81.036702.
- [53] I. Karlin, S. Succi, On the H-theorem in lattice kinetic theory, *Riv. Mat. Univ. Parma* 6 (2) (1999) 143–154.
- [54] S. S. Chikatamarla, I. V. Karlin, Entropy and galilean invariance of lattice boltzmann theories, *Phys. Rev. Lett.* 97 (2006) 190601. doi:10.1103/PhysRevLett.97.190601.
- [55] S. S. Chikatamarla, I. V. Karlin, Lattices for the lattice boltzmann method, *Phys. Rev. E* 79 (4) (2009) 046701. doi:10.1103/PhysRevE.79.046701.
- [56] J. Latt, B. Chopard, Lattice boltzmann method with regularized pre-collision distribution functions, *Math. Comp. Simul.* 72 (2006) 165–168. doi:10.1016/j.matcom.2006.05.017.
- [57] H. Chen, R. Zhang, I. Staroselsky, M. Jhon, Recovery of full rotational invariance in lattice boltzmann formulations for high knudsen number flows, *Phys. A* 362 (2006) 125–131. doi:10.1016/j.physa.2005.09.008.
- [58] R. Zhang, X. Shan, H. Chen, Efficient kinetic method for fluid simulation beyond the navier-stokes equation, *Phys. Rev E* 74 (2006) 046703. doi:10.1103/PhysRevE.74.046703.
- [59] K. Mattila, P. Philippi, L. Hegele Jr., High-order regularization in lattice-boltzmann equations, *Phys. Fluids* 29 (2017) 046103. doi:10.1063/1.4981227.
- [60] A. V. Bobylev, T. Ohwada, The error of the splitting scheme for solving evolutionary equations, *Appl. Math. Lett.* 14 (1) (2001) 45–48. doi:10.1016/S0893-9659(00)00110-5.
- [61] R. J. LeVeque, et al., *Finite volume methods for hyperbolic problems*, Vol. 31, Cambridge university press, 2002.
- [62] C. Baranger, N. Hérouard, J. Mathiaud, L. Mieussens, Numerical boundary conditions in finite volume and discontinuous galerkin schemes for the simulation of rarefied flows along solid boundaries, *Math. Comput. Simul.* 159 (2019) 136–153. doi:10.1016/j.matcom.2018.11.011.
- [63] T. Inamuro, B. Sturtevant, Numerical study of discrete-velocity gases, *Phys. Fluids* 2 (12) (1990) 2196–2203. doi:10.1063/1.857825.
- [64] V. V. Aristov, F. G. Tcheremissine, Conservative splitting method for solving the boltzmann equation, *USSR Comp. Math. Math. Phys.* 20 (1) (1980) 208–225. doi:10.1016/0041-5553(80)90074-9.
- [65] C. Kim, Formation and propagation of discontinuity for boltzmann equation in non-convex domains, *Commun. Math. Phys.* 308 (3) (2011) 641–701. doi:10.1007/s00220-011-1355-1.
- [66] Y. Guo, C. Kim, D. Tonon, A. Trescases, Regularity of the boltzmann equation in convex domains, *Inventiones mathematicae* 207 (1) (2017) 115–290. doi:10.1007/s00222-016-0670-8.
- [67] I.-K. Chen, H. Funagane, T.-P. Liu, S. Takata, Singularity of the velocity distribution function in molecular velocity space, *Commun. Math. Phys.* 341 (1) (2016). doi:10.1007/s00220-015-2476-8.
- [68] I.-K. Chen, T.-P. Liu, S. Takata, Boundary singularity for thermal transpiration problem of the linearized boltzmann equation., *Archive for Rational Mechanics & Analysis* 212 (2) (2014). doi:10.1007/s00205-013-0714-9.

- [69] O. Rogozin, Hybrid finite-volume solver based on the lattice-Boltzmann and discrete-velocity methods for the Couette problem (2019). doi:10.5281/zenodo.3471926.
- [70] W. Li, L.-S. Luo, J. Shen, Accurate solution and approximations of the linearized bgk equation for steady couette flow, *Comput. Fluids* 111 (2015) 18–32. doi:10.1016/j.compfluid.2014.12.018.
- [71] S. Jiang, L.-S. Luo, Analysis and accurate numerical solutions of the integral equation derived from the linearized bgkw equation for the steady couette flow, *J. Comput. Phys.* 316 (2016) 416–434. doi:10.1016/j.jcp.2016.04.011.
- [72] O. Rogozin, Solver for the linear Couette-flow problem for a rarefied BGK gas (2019). doi:10.5281/zenodo.3471914.
- [73] Y. Sone, S. Takata, T. Ohwada, Numerical analysis of the plane couette flow of a rarefied gas on the basis of the linearized boltzmann equation for hard-sphere molecules, *Eur. J. Mech. B/Fluids* 9 (1990) 273–288.
- [74] L. Wu, J. M. Reese, Y. Zhang, Solving the boltzmann equation deterministically by the fast spectral method: application to gas microflows, *J. Fluid Mech.* 746 (2014) 53–84. doi:10.1017/jfm.2014.79.
- [75] O. Rogozin, Numerical analysis of the nonlinear plane couette-flow problem of a rarefied gas for hard-sphere molecules, *Eur. J. Mech. B/Fluids* 60 (2016) 148–163. doi:10.1016/j.euromechflu.2016.06.011.
- [76] F. Sharipov, J. L. Strapasson, Benchmark problems for mixtures of rarefied gases. i. couette flow, *Phys. Fluids* 25 (2) (2013) 027101. doi:10.1017/jfm.2014.79.
- [77] W. Su, P. Wang, H. Liu, L. Wu, Accurate and efficient computation of the boltzmann equation for couette flow: influence of intermolecular potentials on knudsen layer function and viscous slip coefficient, *J. Comput. Phys.* (2018). doi:10.1016/j.jcp.2018.11.015.
- [78] J. Meng, N. Dongari, J. M. Reese, Y. Zhang, Breakdown parameter for kinetic modeling of multiscale gas flows, *Phys. Rev. E* 89 (6) (2014) 063305. doi:10.1103/PhysRevE.89.063305.
- [79] F. Chen, A. Xu, G. Zhang, Y. Li, S. Succi, Multiple-relaxation-time lattice boltzmann approach to compressible flows with flexible specific-heat ratio and prandtl number, *Europhys. Lett.* 90 (2010) 54003. doi:10.1209/0295-5075/90/54003.
- [80] N. Frapolli, S. Chikatamarla, I. Karlin, Entropic lattice boltzmann model for compressible flows, *Phys. Rev. E* 92 (2015) 061301(R). doi:10.1103/PhysRevE.92.061301.
- [81] N. Frapolli, S. Chikatamarla, I. Karlin, Entropic lattice boltzmann model for gas dynamics: Theory, boundary conditions, and implementation, *Phys. Rev. E* 93 (2016) 063302. doi:10.1103/PhysRevE.93.063302.
- [82] V. V. Aristov, Method of adaptative meshes in velocity space for the intense shock wave problem, *USSR Comput. Math. Math. Phys.* 17 (4) (1977) 261–267.
- [83] R. R. Arslanbekov, V. I. Kolobov, A. A. Frolova, Kinetic solvers with adaptive mesh in phase space, *Phys. Rev. E* 88 (6) (2013) 063301. doi:10.1103/PhysRevE.88.063301.
- [84] C. Baranger, J. Claudel, N. Hérouard, L. Mieussens, Locally refined discrete velocity grids for stationary rarefied flow simulations, *J. Comput. Phys.* 257 (2014) 572–593. doi:10.1016/j.jcp.2013.10.014.
- [85] D. R. Willis, Comparison of kinetic theory analyses of linearized couette flow, *Phys. Fluids* 5 (2) (1962) 127–135. doi:10.1063/1.1706585.
- [86] M. Abramowitz, I. A. Stegun, *Handbook of mathematical functions: with formulas, graphs, and mathematical tables*, National Bureau of Standards, 1972.